**The
Propagation
Group**

Georgia Institute
of Technology

Broadband Spatio-Temporal Channel Sounder for the 2.4 GHz ISM Band

Document ID: PG-TR-060831-CJD

Date: 31 August 2006

Christopher J. Durkin,

Ryan J. Pirkl,

Alexander J. Trzecieski,

and Prof. Gregory D. Durgin

Georgia Institute of Technology

Department of Electrical and Computer Engineering

777 Atlantic Ave. Atlanta, GA 30332-0250

CONTENTS

Propagation Group | Georgia Institute of Technology

List of Figures

Propagation
Group Georgia Institute of Technology

List of Tables

EXECUTIVE SUMMARY

This report documents the continuing research efforts of the Propagation Group at Georgia Tech towards the construction of a broadband spatio-temporal channel sounder for the Aerospace Corp. The channel sounder, a valuable research tool in radio frequency (RF) channel and direction finding (DF) measurement, was constructed from the 8-element antenna array receiver setup on loan from Aerospace Corporation to support this collaborative project.

Upon completion of the 2006 portion of this on-going collaboration, the following contributions were made to the system:

■ The broadband *pseudo-random noise generator* was modified for improved operation and wider bandwidth.

■ The *vector RF signal generator* was improved to be cleaner, more stable, and include onboard programming firmware, obviating the need for an external computer and allowing better transmitter portability.

■ An autonomous self-powered transmitter platform was constructed.

■ Extensive improvements were made to the RF receiver signal chain in order to compensate for near out-of-band interference and amplifier noise.

■ Software improvements included an SQL database interface for captured data and associated metadata in order to facilitate storage and retrieval.

In addition to these improvements, field measurements were taken to demonstrate channel sounding operation and direction finding in environments with copious noise and interference. Collectively, these outputs fulfill the research deliverables for the year 2006 collaborative project between Aerospace Corporation and Georgia Tech.

Future work for this ongoing collaboration will likely involve more measurements and further miniaturization of the array channel sounder. The ultimate goal of the research should be a single compact receiver box containing all RF components and analog-to-digital conversion hardware. This

box could then be plugged into a network or laptop computer and an arbitrary array manifold for portable direction-finding and channel measurement. When coupled with the array processing software developed during the 2004 and 2005 phase of this collaborative project, the end result will be a dynamic, portable unit capable of both spatio-temporal channel sounding and/or accurate DF location of 2.4 GHz radios in a complicated radioscape. Temporal and spatial analysis of the measurements should be able to yield detailed data to assist in detailed channel characterization.

**Propagation
Group**

Chapter 1

INTRODUCTION

This technical report describes the continued improvement of a broadband spatio-temporal channel sounder operating at the 2.4 GHz ISM frequency band, as well as a measurement campaign demonstrating the sounder. Based on the core 8-element receiver system provided by the Aerospace Corp., Georgia Tech graduate student researchers Chris Durkin and Ryan Pirkl designed new hardware and software that allows broadband RF channel sounding with increased mobility for measurement. Key contributions include an improved high-speed *pseudo-random noise (PN) generator* for transmitting a broadband waveform, an improved *vector RF signal generator* for generating stable, programmable frequencies to drive receiver hardware, improved filtering in the RF receiver front end, and spatio-temporal data acquisition software.

This work is a continuation of the direction-finding research collaboration conducted by the Aerospace Corp. and the Propagation Group at the Georgia Institute of Technology. The new channel sounding system is capable of resolving multipath delay spread of 100 ns of time-of-arrival delay.

1.1 Motivation

All terrestrial direction-finding (DF) receivers must contend with the distorting effects of multipath propagation as well as the ever-increasing number of in-band radio interferers. This is especially true when ranging mobile wireless terminals such as those operating in the 2.4 GHz *industrial-scientific-medical* (ISM) band, which operate in high multipath, high interference environments.

The combination of broadband channel sounding capability with the 8-element receiver array is a powerful research tool for illuminating the spatio-temporal characteristics of the radio channel at 2.4 GHz. PN correlations may then be performed in software to extract channel information as a function of delay; direction finding (DF) algorithms may simultaneously be performed in software to extract spatial channel information.

Not only are conventional space-time statistics (angle-of-arrival, time-of-arrival, delay spread, angle spread, etc.) available with such measurements, but we propose a new technique for extracting

Propagation
Group [Georgia Institute of Technology]

3

multipath characteristics from within a measured delay "bin". Each delay "bin" contains a variety of multipath components which will produce small-scale fading in space. An example of such broadband fading is illustrated in Figure 1.1.
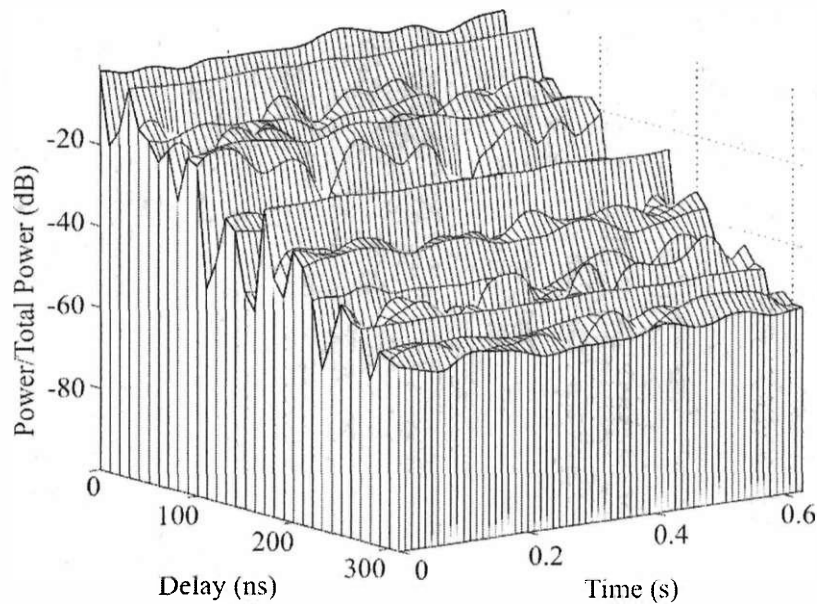
Figure 1.1 Example of a broadband channel fading as a function of motion. The delay samples undergo different levels of Rician fading, revealing the underlying multipath structure of the channel [Dur03].

Usually, the intra-bin multipath consists of one or two dominant, specular wave components and a group of smaller multipath waves that can collectively be regarded as *diffuse* power. By dragging the receiver antennas through space, it is possible to collect a histogram of fading power for each delay "bin". The unique shape of the histogram will illuminate the underlying multipath structure [Abd00], [Dur02].

1.2   Future Work

In 2004, the collaboration between Aerospace Corp. and Georgia Tech resulted in a suite of software capable of analyzing the various direction-finding algorithms for measurement data. In 2005, the collaboration resulted in a working spatio-temporal channel sounder with an 8-element array. In 2006, further improvements to the system were made and interesting measurements were conducted in the 2.4 GHz band.

Future work should focus on the following areas:

■ Transmit orthogonal PN codes to measure MIMO channel characteristics

■ Incorporate GPS into the transmitter system

■ Transmitter location prediction using delay spread and DF algorithms, and verification from GPS data

■ Integrate RF front end with improved filtering onto a single PCB

Chapter 2

HARDWARE

2.1 Changes to Receiver

Previous measurements made using the system were taken indoors. However, the multipath propagation delays (on the order of tens of nanoseconds) were of insufficient duration to measure with the available receiver bandwidth. Once the system was moved outside, near out-of-band interference was found to be saturating the input LNAs. ISM band RF filters were present in the receiver signal chain, but only after the LNA, so these filters were moved directly after the antenna. In addition, HPFs were added in both the RF and IF sections of the receiver to further mitigate the effects of near out-of-band interference. See Figure 2.1 for a revised system block diagram. To summarize, the following were added:

- Pre-LNA filtering, confining all signals entering the LNA to the 2.4 GHz ISM band.

- High-pass filtering of the RF signal and IF signal. The previous design contained low-pass filtering only and did not properly constrain the unambiguous bandwidth.

2.2 Power calibration

System calibration provided linear correlation between the ADC 8-bit integer value and the received signal voltage. The transmitter output power was first measured directly using a spectrum analyzer. Then, the output was connected to the receiver via a stepped-attenuator. The attenuator was stepped from 0 to 70 dB in 10 dB increments. The ADC range was 0 to 255 bits, creating a DC term that necessitated removal prior to processing. The zero-mean ADC data, which represented scaled voltage, was squared to represent scaled power. This scaled power was plotted against true power to identify the linear region of operation. Within this region, a constant correction factor was applied to align the measured power with the true power. The nonlinear region received the same correction factor.

The resulting curve shows a 1 to 1 relationship between measured power and true power for the

Propagation
Group
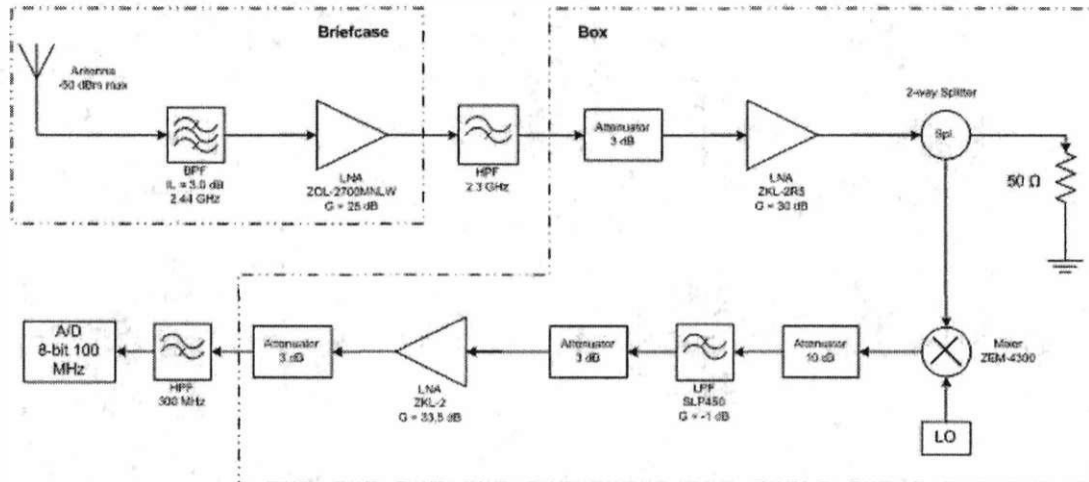
Figure 2.1 Revised receiver block diagram.
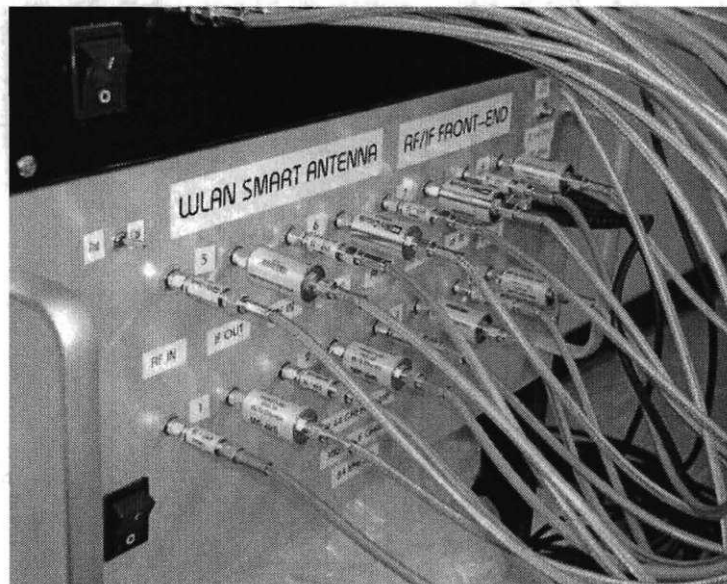
Figure 2.2 Photograph of the added filtering.

range of -85 dBm to -55 dBm as shown in Figure 2.4. Above -55 dBm, the receiver's amplifiers become saturated. Therefore, the received signal power should be no more than -55 dBm to ensure

Figure 2.3 Photograph of LNA pre-filtering modifications.

that the receiver is operating in the linear region.
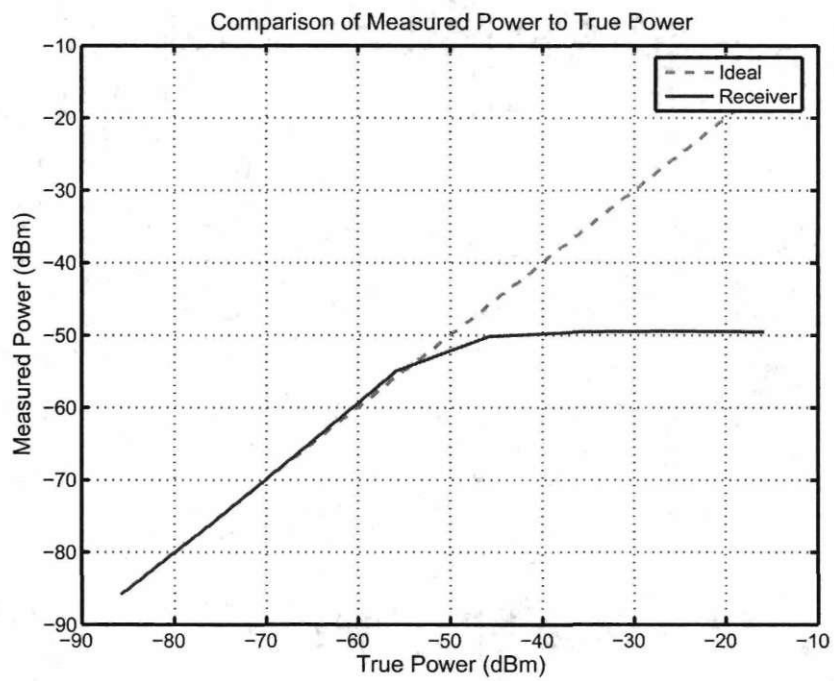
Figure 2.4 Comparison of power measured using receiving hardware to power measured with a spectrum analyzer.

Chapter 3

RECEIVER PN PROCESSING

The following section gives some background on the receiver PN processing used to produce delay spread measurements. Discussion of channel characteristics draws mainly from [Dur03].

3.1 Despreading

After shifting the signal to baseband, and thereby generating the inphase and quadrature channels, it is necessary to despread the signal. Despreading is achieved via cross-correlation of the signal with a template pseudo-random noise (PN) sequence that is identical to the transmitted PN. Figure 3.1 shows a section of a PN sequence.

The binary PN sequence was generated in software by emulating the Fibonacci topology for a linear feedback shift register (LFSR) [Gor02]. The resulting binary sequence was then "clocked" at 10 MHz, sampled at 99 MHz, and normalized. Excepting phase offsets, this generates a digitized copy of the transmitted baseband signal with unit power.

Assuming two wide-sense stationary processes $x(t)$ and $y(t)$, cross- correlation in the time domain is defined as

$$R_{xy}(\tau) = \int x(t)y(t - \tau)dt \tag{3.1.1}$$

Similarly, in the discrete domain, the cross-correlation is

$$R_{xy}(m) = \sum_{n=1}^{L} x(n)y(n - m) \tag{3.1.2}$$

Cross-correlation of the discretized baseband received signal with this template PN serves to despread the spread spectrum signal, and thereby significantly reducing its bandwidth. The template PN acts as a matched filter for the transmitted PN sequence, selectively extracting it and compressing its spectrum while suppressing any noise or interferers that may be present. This entire operation provides an improvement in the signal-to-noise ratio, which is defined as the ratio of signal power to noise power:

$$SNR = \frac{\langle |s(t)|^2 \rangle}{\langle |n(t)|^2 \rangle} \tag{3.1.3}$$

Section of Template PN Sequence
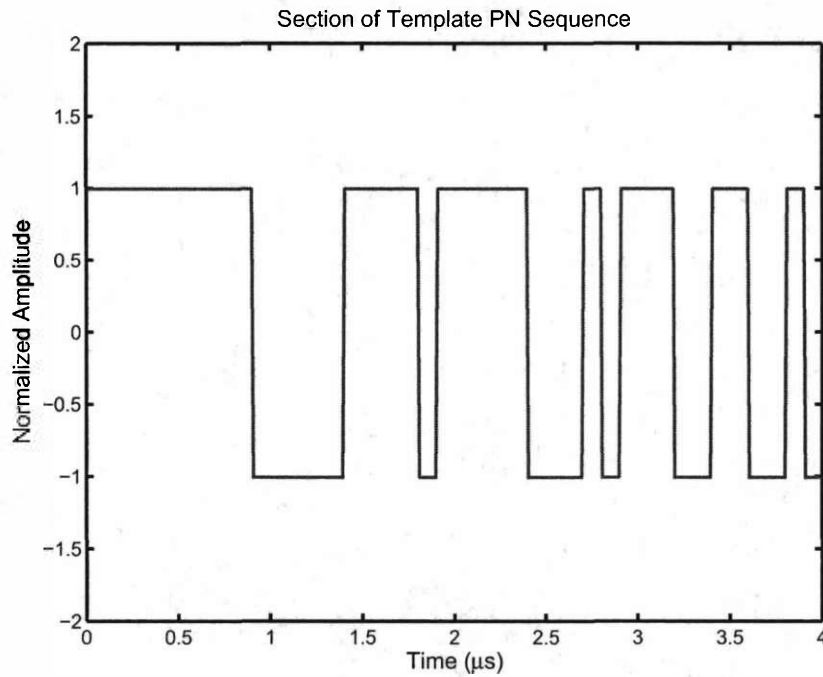
Figure 3.1 Section of a 511-bit PN sequence clocked at 10 MHz.

Assuming white Gaussian noise, then

$$SNR = \frac{\langle |s(t)|^2 \rangle}{N_0 BW} \tag{3.1.4}$$

where N_0 is the noise power density and BW is bandwidth.

It can be seen from 3.1.4 that the wider the bandwidth, the greater the total noise power present in a system. For example, consider two signals with equal signal power. However, one signal occupies twice the bandwidth of the other. For a given receiver with a constant noise figure, the narrow-band signal would have twice the SNR as compared to its more wide-band cousin. If one could somehow compress the spectrum of the wide-band signal without losing any signal power, then the SNR would improve accordingly.

Therefore, the reduction in bandwidth brought about by despreading the received signal leads to an improvement in the SNR. This change in SNR due to despreading is known as process gain and, for direct sequence spread spectrum systems, may be estimated as [Dix94]

$$G_p = \frac{SNR_{out}}{SNR_{in}} \approx \frac{\frac{P_R}{BW_{out}}}{\frac{P_R}{BW_{in}}} = \frac{BW_{in}}{BW_{out}} = \frac{BW_{RF}}{R_{data}} \tag{3.1.5}$$

Propagation Group [Georgia Institute of Technology]

For direct sequence spread spectrum systems, the data rate R_{data} assuming utilization of the both inphase and quadrature RF channels is [Dix94]

$$R_{data} = 2\frac{f_{clk}}{L} \qquad\qquad (3.1.6)$$

where L is the length of the PN sequence.

There are various metrics for calculating the bandwidth of a direct sequence spread spectrum signal depending on whether one uses the -3 dB bandwidth, the -10 dB bandwidth, or the null-to-null bandwidth. As a matter of simplicity, this report will use the convention of null-to-null bandwidth, which is easily shown to be twice the clock rate of the PN sequence. Figure 3.2 shows the spectrum of a PN sequence; note the nulls occur at ±10 MHz.
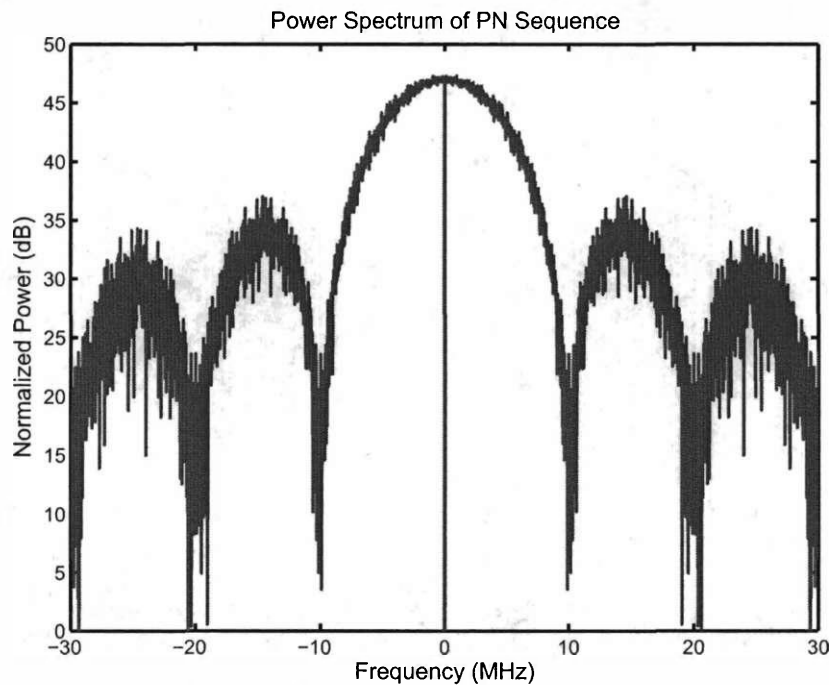
Figure 3.2 Spectrum of a 511-bit PN sequence clocked at 10 MHz.

Accordingly, given that $BW_{RF} = 2f_{clk}$, it can be seen from 3.1.5 and 3.1.6 that the processing gain of a direct sequence spread spectrum system is equivalent to the length of the PN sequence. While larger codes provide greater processing gain, they also require additional time to transmit the entire sequence. The longer signal period can be compensated by increasing the clock rate of the PN sequence, but this will in turn require more bandwidth in the RF link and, due to system constraints and FCC regulations, such bandwidth may not always be available.

Propagation Group Georgia Institute of Technology

August 30, 2006

3.2   Infinite bandwidth channel impulse response

For a channel of infinite bandwidth, the CIR is the complex response of the channel to a transmitted signal such that

$$\tilde{x_R}(t) = \tilde{H}(\tau; t, r) \otimes x_T(t) \tag{3.2.1}$$

where $\otimes$ denotes convolution, $x_T(t)$ is the transmitted baseband voltage waveform, $\tilde{x_R}(t)$ is the received quadrature waveform, and $\tilde{H}(\tau; t, r)$ is the baseband representation of the CIR at time t and location r, and represents the Fourier transform pair of the wireless channel $h(t, f, r)$ with respect to frequency. It should be pointed out that the definition of the wireless channel $h(t, f, r)$ is for the pass-band representation, meaning that the frequency f corresponds to the actual radio frequency of interest. However, it is generally more convenient to work in baseband.

It should be further noted that the convolution described in 3.2.1 applies to delay, τ, with respect to the channel impulse response and time, t, with respect to the transmitted signal. This becomes more digestible for the case of a static channel, for which one may ignore the temporal variations. Therefore

$$\tilde{x_R}(t) = \tilde{H}(\tau; r)\Big|_{\tau=t} \otimes x_T(t) \tag{3.2.2}$$

where it is becomes more apparent that the convolution operator applies to the parameters in $\tilde{H}(\tau; r)$ and $x_T(t)$ that carry the units of time: τ and t, respectively. To minimize confusion, the assumption of a static channel will be made to make the math more lucid. Justification of this assumption shall follow in a later section.

Mathematically, the CIR may be described as a summation of Dirac delta functions, each with a delay τ_i and complex amplitude $\tilde{A}_i$.

$$\tilde{H}(\tau; r) = \sum \tilde{A}_i \delta(\tau - \tau_i) \tag{3.2.3}$$

An example of a CIR can be seen in Figure 3.3. Convolution of the transmitted signal with the CIR produces a received signal $\tilde{x_R}(t)$ at location r that is equivalent to the sum of multiple delayed and complex-scaled copies of $x_T(t)$.

$$\tilde{x_R}(t) = \tilde{H}(\tau; r)\Big|_{\tau=t} \otimes x_T(t) = \sum \tilde{A}_i x_T(t - \tau_i) \tag{3.2.4}$$

Therefore, if one were to transmit a waveform defined as an impulse function scaled by a voltage V_T

$$x_T(t) = V_T \delta(t) \tag{3.2.5}$$

then the received waveform $\tilde{x_R}(t)$ would represent the CIR scaled by the voltage V_T at location r.

$$\tilde{x_R}(t) = V_T \, \tilde{H}(\tau; r)\Big|_{\tau=t} \tag{3.2.6}$$

Normalization of the received waveform by V_T would therefore result in the CIR.

Propagation Group [Georgia Institute of Technology]
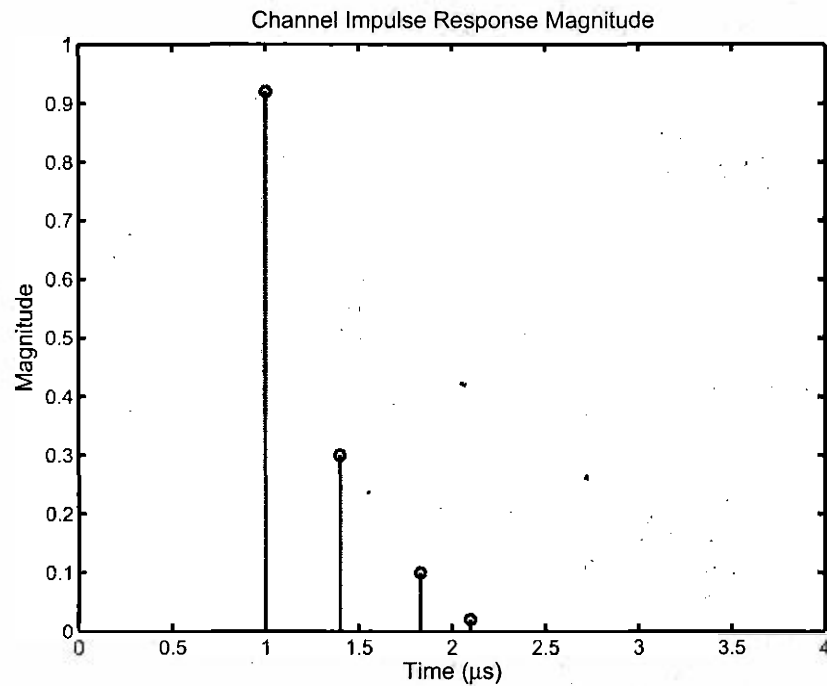
Channel Impulse Response Magnitude

Figure 3.3 Example channel impulse response.

3.3   Band-limited channel impulse response

The description of the CIR as a summation of delayed, complex impulses assumes a channel of infinite bandwidth. The Fourier transform of an impulse $\delta(t)$ scaled by $\tilde{A}$ and delayed by τ has constant magnitude and frequency dependent phase.

$$F\{\tilde{A}\delta(t-\tau)\} = \tilde{A}e^{j2\pi f\tau} \tag{3.3.1}$$

Any constant term spanning the entire frequency domain is commonly referred to as white noise, and it is this infinite bandwidth that leads to the infinitesimally short impulse in the time domain. Physical and practical limitations on bandwidth make it impossible to sound a wireless channel with a truly infinite bandwidth impulse. However, it is possible to transmit and receive a band-limited impulse as approximated by a short duration waveform, such as a square wave.

The PN template sequence consists of a train of square waves with duration T_c, as given by

$$pn(t) = \sum_{i=1}^{L} V_i rect(T_c, t - T_c(i - 1/2)) \tag{3.3.2}$$

**Propagation
Group** [Georgia Institute of Technology]

and

$$rect(T, t) = u(T/2 - |t|) \qquad\qquad (3.3.3)$$

where $u(t)$ is the unit step function, L is the length of the PN sequence, V_i is -1, 1 as determined by the PN sequence, and T_c is the period given as $1/f_{clk}$. For the purpose of channel sounding, the transmitted signal may be described as a single square wave with amplitude V_T as shown in Figure 3.4.

$$x_T(t) = V_T rect(T_c, t - T_c/2) \qquad\qquad (3.3.4)$$

In reality, a train of such square waves are being transmitted in a pseudo-random pattern such that the train of pulses as a whole resemble band-limited white noise. More precisely, the spectrum of the PN sequence appears as white noise bounded by the spectral mask corresponding to a $sinc(T_c f)$ function as seen in Figure 3.2. Thereby, the transmitted PN sequence is band-limited white noise, from which it becomes possible to determine the band-limited channel impulse response. Again
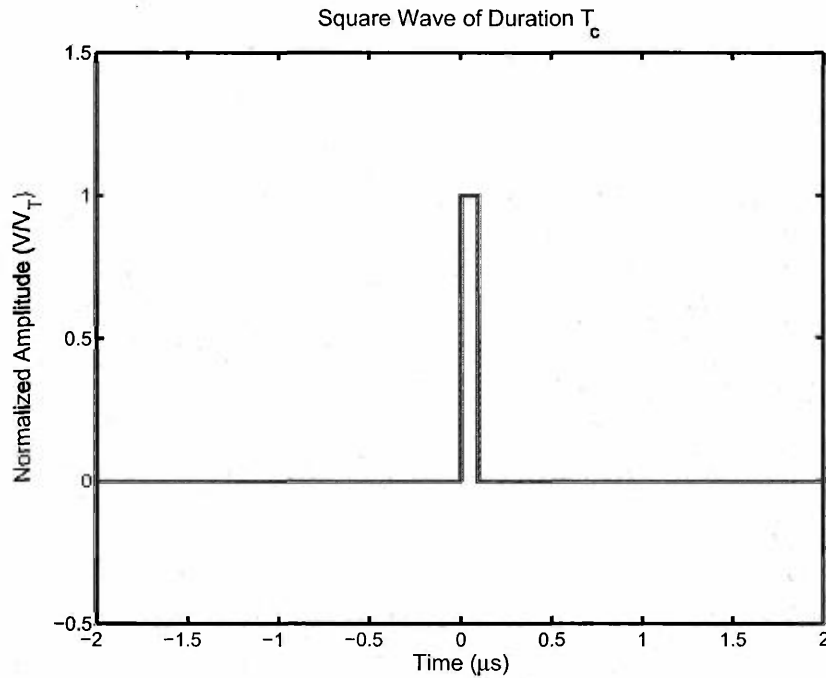

Figure 3.4 The band-limited impulse with duration T_c used for channel sounding.

considering the transmission of a single square wave, the received waveform will be

$$\tilde{x}_R(t) = \sum [\tilde{A}_i V_T rect(T_c, t - T_c/2 - \tau_i)] \qquad\qquad (3.3.5)$$

which is the summation of a train of complex-scaled and delayed square waves as resulting from the convolution of the transmitted waveform with the CIR as seen in Figure 3.5. Cross-correlation of $\tilde{x}_R(t)$ with a unit amplitude template of the transmitted square wave $x_T(t)$ produces a corresponding train of complex-scaled and delayed triangles waves.
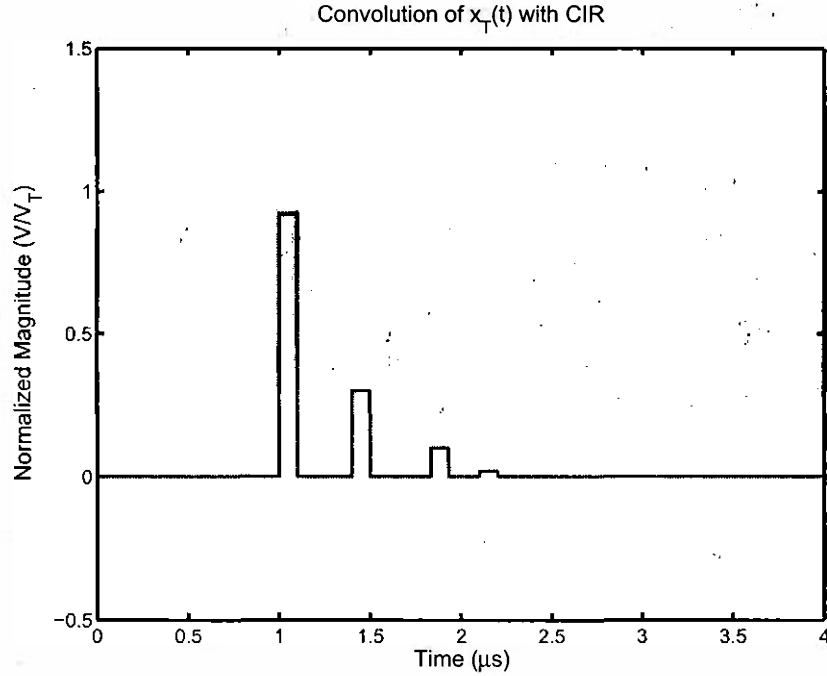

Figure 3.5 The convolution of the band-limited impulse with the example channel impulse response.

$$R_{x_Rpn}(\tau) = \sum[\tilde{A}_i V_T T_c triangle(2T_c, t - \tau_i - T_c/2)] \tag{3.3.6}$$

where

$$triangle(T, t) = (1 - 2|t|/T)rect(T, t) \tag{3.3.7}$$

The cross-correlation operation acts as a matched filter and further contributes to the band-limited nature of the CIR by imposing yet another spectral mask corresponding to $sinc(T_c f)$. Therefore, the entire impulse response is band-limited by $sinc(T_c f)^2$, which in the time domain corresponds to $triangle(T_c, t)$. Thus, the band-limited CIR becomes the convolution of the infinite bandwidth CIR with $triangle(2T_c, t)$.

$$\tilde{H}_{BL}(\tau; r) = \tilde{H}(\tau; r) \otimes triangle(2T_c, t) = \sum \tilde{A}_i triangle(2T_c, t - \tau_i) \tag{3.3.8}$$

This is precisely the result that is achieved after the cross-correlation product is normalized by the transmit waveform voltage V_T and the square- wave duration T_c.

Switching from the square-wave to a PN sequence consisting of a train of square-waves, the end result differs only in the normalization. Considering the PN sequence as long square wave of duration LT_c, where L is the length of the PN sequence, it can be seen that this will simply scale the cross-correlation product by a factor L. This is the realization of the processing gain afforded by a PN sequence as discussed previously. Therefore, normalization of the cross-correlation product by the transmit waveform voltage V_T and PN period LT_c will produce the band-limited CIR as seen in Figure 3.6. Figure 3.7 shows a measured channel impulse response produced by the aforementioned method.
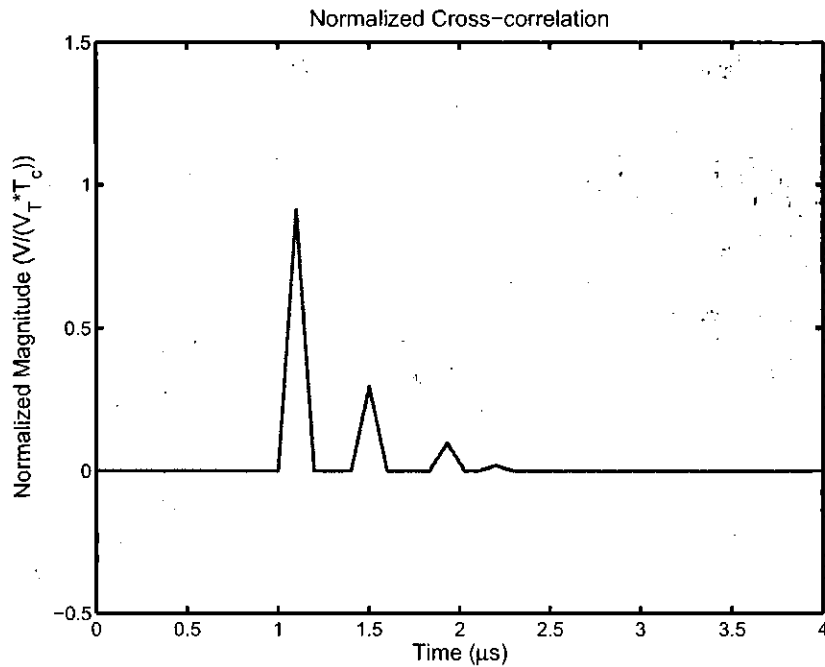

Figure 3.6 The normalized cross correlation of the received waveform with the template PN sequence.

$$\tilde{H}_{BL}(\tau; r) = \frac{R_{x_H pn}(\tau)}{V_T LT_c} \tag{3.3.9}$$
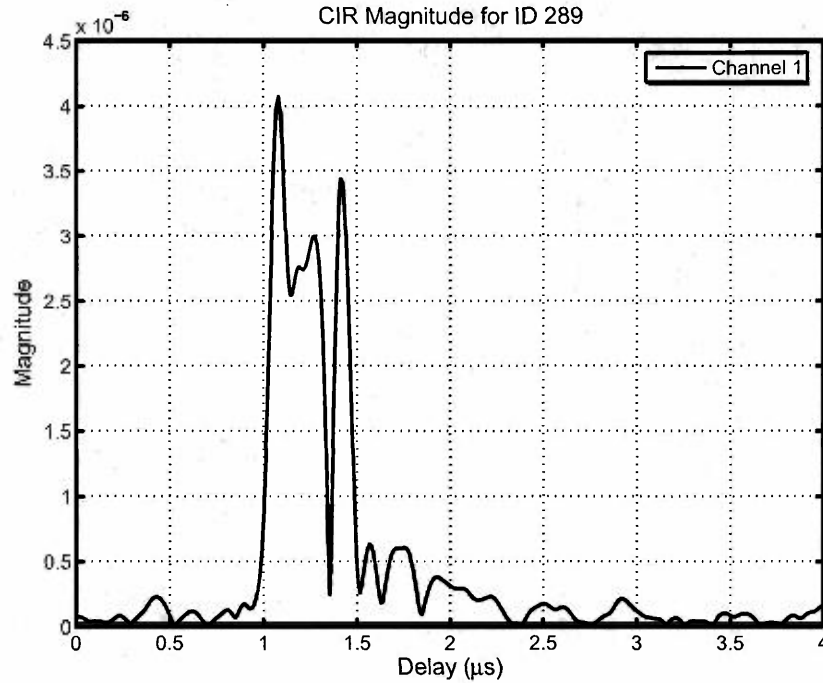
**Propagation
Group**

Figure 3.7 The measured channel impulse response for ID 289.

3.4 Power delay profile

A more common representation of the time-delayed multipath is the power delay profile (PDP), which is defined as the magnitude-squared of the CIR.

$$PDP = |\tilde{H}(\tau; r)|^2 \tag{3.4.1}$$

The PDP is the path loss through the channel and is typically expressed in dB. The envelope of a PDP generally follows an exponential decay curve, with the strongest multipath components (typically the line-of-sight component) arriving earliest, followed by weaker multipath components with increased delay. This is not an absolute statement however, and depending on the physics of the channel, weaker multipath components can arrive before stronger ones.

3.5 Time averaged power delay profiles

The measurements (see Chapter 5) were performed on a university campus between semesters late at night. These conditions, as well as the zero velocity of both transmitter and receiver, make for a mostly static channel. However, time-varying scatterers caused by trees swaying in the wind
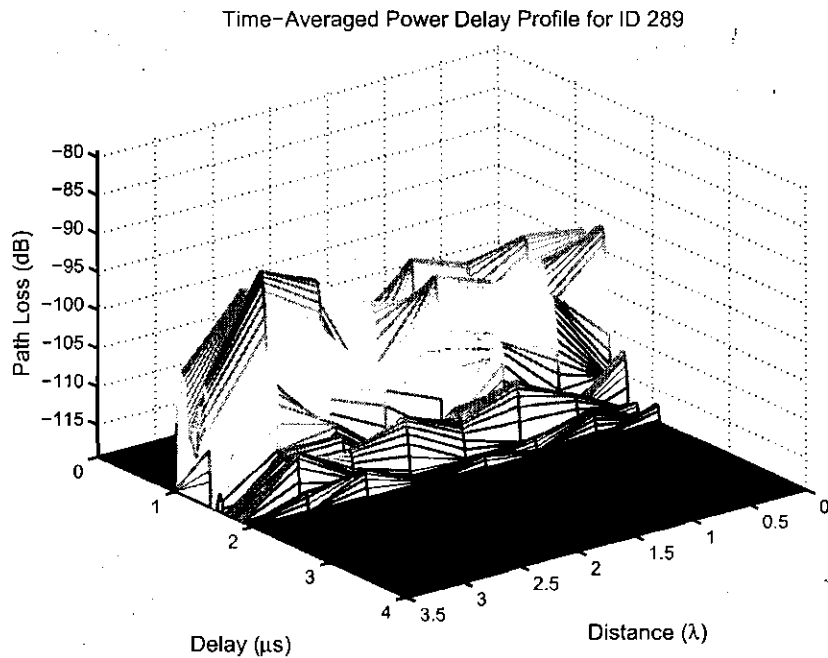
Time-Averaged Power Delay Profile for ID 289

Figure 3.8 Power delay profile for ID 289.

as well as the occasional moving vehicle or pedestrian can effect magnitude, phase, and delay of multipath components, introduce additional multipath, and produce a non-zero Doppler spectrum. The relatively slow temporal variations afforded by these scatterers would have minimal effect on the channel characteristics during the short sampling period employed in this measurement campaign and time-averaging of the PDP with respect to time would remove any such perturbations. Figure 3.8 shows a measured power delay profile after time-averaging.

3.6 Delay spectrum

The delay spectrum is the power spectral density of the channel as a function of delay and is the source of several key channel parameters such as RMS delay spread and coherence bandwidth. The delay spectrum $S_h(\tau)$ is defined as the Fourier transform of the autocorrelation of the channel's frequency response,

$$S_h(\tau) = F\left\{E\{h(f)h(f + \Delta f)\}\right\} \tag{3.6.1}$$

or equivalently,

$$S_h(\tau) = |\tilde{H}(\tau)|^2 \tag{3.6.2}$$

Therefore, the delay spectrum is the expectation of the path loss through a wireless channel at a given delay. It is important to note the absence of the now familiar space parameter r that was present in the CIR and PDP. The delay spectrum represents the expected path loss at any point within the channel. This differs from the PDP, which is the actual path loss at a given point within the channel. Such a localized measurement is susceptible to the rapid spatial variations in the wireless channel.

While physical fluctuations within the channel lead to temporal variations in multipath power, the very physics of the channel lead to spatial variations and thereby spatial selectivity. For the pedagogical case of free space, the propagation of a single homogeneous plane wave through a region devoid of scatterers will result in a uniform power density within the region. Compare this to the propagation of two homogeneous plane waves with identical polarizations but unique wave vectors. The electric fields of the plane waves will constructively and destructively interfere, resulting in a spatially varying power density. Therefore, concerning the real world scenario of multipath propagation, which involves numerous homogeneous plane waves with unique delays, wave vectors, and complex amplitudes, spatial channel variations are unavoidable and lead to rapid and dramatic fluctuations in received power. These fluctuations, which are known as small-scale fading, can easily disrupt a wireless link if compensatory techniques such as antenna diversity are not utilized.

If one can assume the wireless channel to be ergodic with respect to space, then spatial averaging of the measurement data will smooth out these fluctuations caused by small-scale fading. For the channel to be ergodic, the spatial average of a given realization of the wireless channel must equal its expected value at any point in space. Thereby

$$\langle |\tilde{H}(\tau;x)|^2 \rangle_x = E\{|\tilde{H}(\tau;x)|^2\}_x \tag{3.6.3}$$

If one can show that the channel meets the criteria for a stochastic local area channel with uncorrelated phases and heterogeneous scattering, then ergodicity with respect to space is implicit,an assumption will be justified.

A stochastic local area channel is defined as a region in which the wireless channel can be accurately described by a summation of homogeneous plane waves. This is typically the case in regions far from scatterers. The second requirement is that the phases of the homogeneous plane waves are uncorrelated. Considering that the many homogeneous plane waves result from different scatterers and travel different distances, it is a safe assumption that their phases will be uncorrelated when they arrive at the receiver antenna.

The requirement of heterogeneous scattering states that no two homogeneous plane waves arrive from the same direction or with the same delay. Given the richness and physical complexity of a propagation environment, while possible, it becomes highly improbable for two waves to arrive at exactly the same time or from exactly the same direction. Finally, ergodicity may only be assumed

for a region defined as the local area. According to the bandwidth-distance threshold, the local area L_A is bounded by the ratio of propagation velocity to bandwidth[Dur03].

$$L_A < C/B \tag{3.6.4}$$

Thereby, all points within L_A of each other can be considered within the same local area. For the measurements presented here, where a null-to-null RF bandwidth of 20 MHz was used, the local area is found to be 15 m, which is considerably larger than the distance separating points at individual measurement locations. Figure 3.9 shows a measured delay spectrum.
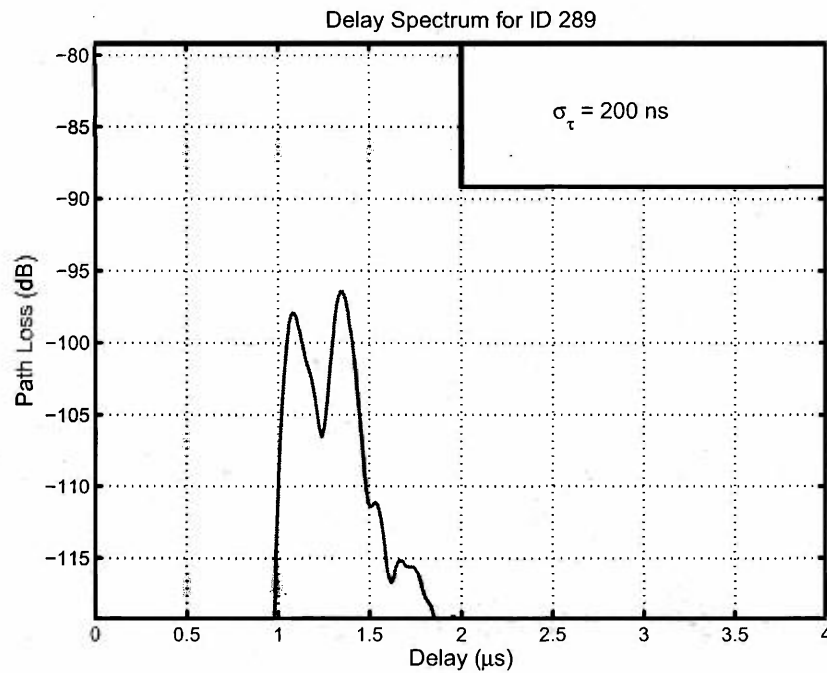
Figure 3.9 The measured delay spectrum for ID 289.

3.7   Channel statistics

Using the delay spectrum, one may extract the RMS delay spread, which is defined as

$$\sigma_\tau = \sqrt{\overline{\tau^2} - (\overline{\tau})^2} \tag{3.7.1}$$

where $\overline{\tau^2}$ and $\overline{\tau}$ are respectively the first and second moments of the delay spectrum. The RMS delay spread is a measure of the frequency selectivity of the wireless channel. Small delay spreads indicate

a large coherence bandwidth, meaning that the frequency response is mostly constant within the spectrum of interest. Conversely, large delay spreads indicate a small coherence bandwidth and thereby a nonuniform frequency response in the spectrum of interest. The coherence bandwidth may be estimated as

$$B_c = 1/5\sigma_\tau \qquad (3.7.2)$$

For the delay spectrum corresponding to location 289, the delay spread σ_τ was 200 ns; the coherence bandwidth was 1 MHz.

Chapter 4

BANDPASS SAMPLING

4.1 Introduction

The RF receiver used in the channel sounder described in this report uses *bandpass sampling* to digitize the incoming real IF signal into a complex baseband representation (see chapter 3 of [Lib99] for a more rigorous treatment). There are several issues related to this approach that are presented in this section.

4.2 Overview

Bandpass sampling is an alternative to mixing a signal down to baseband before sampling. In baseband sampling, two analog-to-digital converters (ADCs) and a 90° phase shifter are required, resulting in two real digital signals, the in-phase and quadrature components.

However, the signal may be digitized while not centered at zero frequency. The resulting real signal still contains both the in-phase and quadrature components. Because the signal is digitized above baseband, the in-phase and quadrature channels can be extracted in software while using a single ADC per channel. It also avoids offset errors in the demodulator and eliminates additional oscillator and mixing hardware. The major drawback to this approach is the extra bandwidth required – typically 2 to 3 times the bandwidth that would be required to digitize the same signal at baseband.

4.3 Theory

Passband sampling depends on the phenomenon of *aliasing* in order to capture a signal that exists at a much higher frequency than the ADC sampling frequency. Most of the time a digital waveform is assumed to have been low-pass filtered to confine the input signals to one half the sampling frequency (the *Nyquist frequency*). Any input signals higher than this frequency cannot be unambiguously reconstructed.

Propagation Group — Georgia Institute of Technology

4.4   Filtering

The Nyquist frequency requirement in normal sampling does not limit the frequency of the input signal; it is more general to say that it constrains the *bandwidth*. Normally it is assumed that the input signal bandwidth is centered at baseband, so it is proper to constrain the signal to the Nyquist frequency and then low-pass filter it. Most ADCs also have limited bandwidth and may end up low-pass filtering the signal anyway.

However, if the input signal bandwidth of the ADC is sufficiently high, the desired bandwidth can be specified as centered on any integer multiple of the sampling frequency, provided that everything outside this bandwidth is filtered out. Hence, a band-pass filter is required before the input to the ADC in order to ensure unambiguous reconstruction. The filter should have bandwidth equal to the bandwidth of the ADC and be centered on the IF frequency of interest.

4.5   Conclusion

As with any receiver system, adequate filtering is of paramount importance. In passband sampling receivers, this includes a tight enough bandpass filter to unambiguously confine the IF signal to the band of interest.

Chapter 5

MEASUREMENT CAMPAIGN

A set of outdoor measurements were taken over a 0.5 mile path on the Georgia Tech campus Figure 5.1. They included measurements of line-of-sight transmission, obstruction by trees and buildings, and areas subject to multi-path through ground and building bounces.
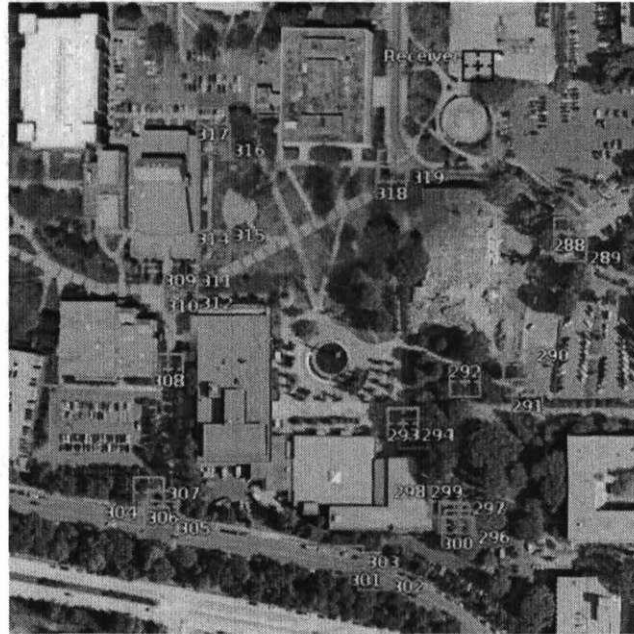
5.1 Map

Signal waveforms were recorded by the receiver, located on the roof of the Van Leer building, from 30 distinct locations in the surrounding area. The 1W transmitter antenna was a monopole located approximately 2 meters above the ground. The measurements were taken on a clear evening in August, with minimal vehicle and pedestrian traffic.

5.2 Phase error correction

Phase errors between the channels must be corrected in order to perform beam steering or direction finding. When injected with a constant phase input signal, the channels were not in phase, but the relative phase deviation was found to be consistent within a few degrees from measurement to measurement, and thus can be largely corrected. Table 5.1 shows the phase deviations for each channel referenced to channel 1.

5.3 Analysis of campaign

Direction finding (DF) and angular and delay spread analysis are currently underway, as well as investigations into the possible signal processing that could be performed upon the data to yield useful results. Future reports and/or papers will detail this work. Preliminary DF plots are provided in Figure 5.4 and Figure 5.5. Figure 5.4 shows the MUSIC ([Sch86]) spatial spectrum as a function of baseband frequency before demodulation, while Figure 5.5 shows the DF MUSIC spectrum of the same data after despreading and demodulation. The processing gain shows clear improvement in locating the line-of-sight component, though multipath components are not evident.

Propagation
Group

Figure 5.1 Map of measured locations. The receiver is on the rooftop in the top right. (Image produced using Google Earth, 2006)

Ch 1	Ch 2	Ch 3	Ch 4	Ch 5	Ch 6	Ch 7	Ch 8
0.0	20.7	16.3	13.9	9.7	11.4	29.3	31.4
0.0	20.8	15.5	14.0	10.1	11.9	29.8	31.9
0.0	20.8	12.5	13.8	9.9	11.8	29.7	31.7
0.0	20.7	15.4	13.8	9.7	11.7	29.3	31.4
0.0	18.5	13.9	13.5	10.8	8.8	29.7	29.5
0.0	18.5	12.5	13.5	10.8	8.7	29.5	29.3
0.0	18.6	14.3	13.5	10.8	8.7	29.5	29.3
0.0	18.6	11.9	13.6	10.8	8.7	29.6	29.4

Table 5.1 Relative phase deviation (in degrees) for a 2.44 GHz calibration tone, eight instances. The first four were taken immediately before the field measurements, the last four immediately after.
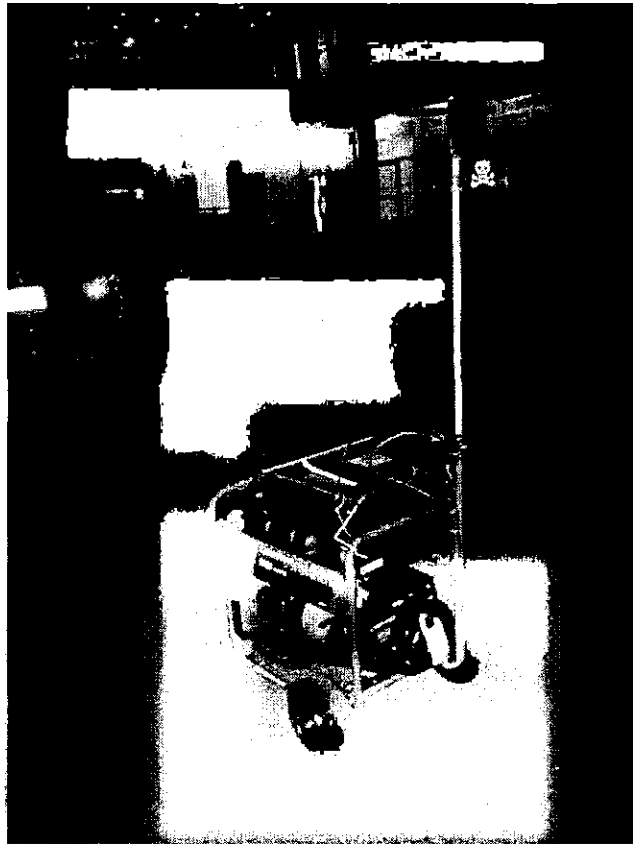
Figure 5.2 The receiver system on the roof.
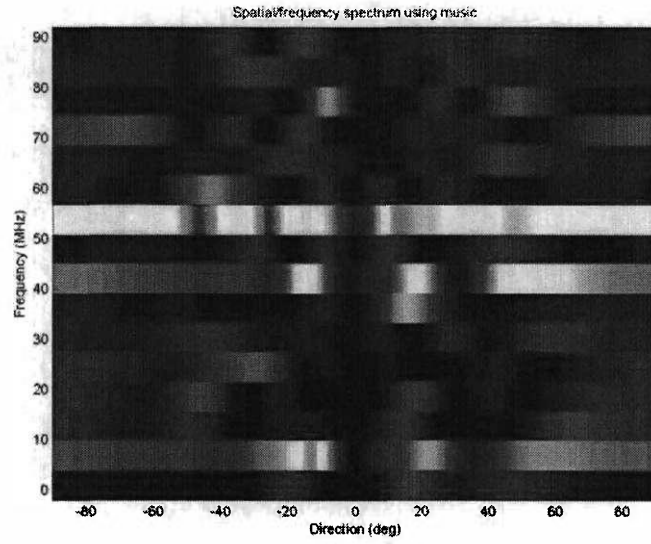
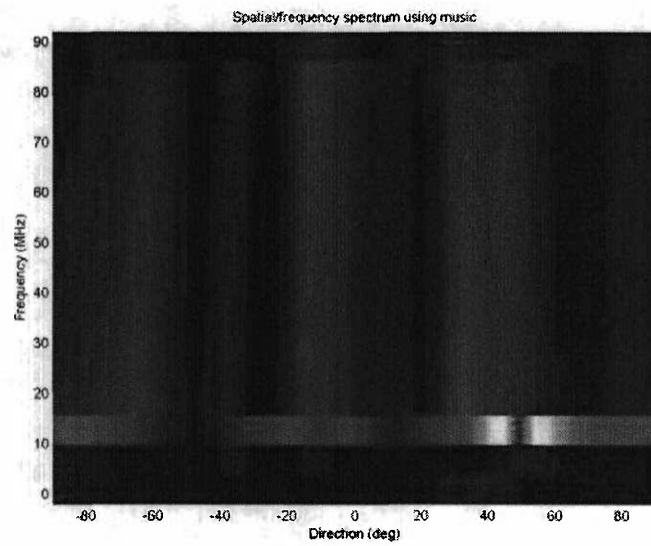Figure 5.3 The transmitter in the field.

Figure 5.4 Raw DF spectrum.

Figure 5.5 DF spectrum after despreading and demodulation.

BIBLIOGRAPHY

[Abd00] A. Abdi, H. Hashemi, and S. Nader-Esfahani, "On the PDF of the Sum of Random Vectors," *IEEE Transactions on Communications*, vol. **48**, no. 1, pp. 7–12, Jan 2000.

[Dix94] R. C. Dixon, *Spread Spectrum Systems with Commerical Applications*, John Wiley and Sons, Inc., 1994.

[Dur02] G.D. Durgin, T.S. Rappaport, and D.A. de Wolf, "New Analytical Models and Probability Density Functions for Fading in Wireless Communications," *IEEE Transactions on Communications*, vol. **50**, no. 6, pp. 1005–1015, June 2002.

[Dur03] G.D. Durgin, *Space-Time Wireless Channels*, Prentice Hall Inc., Upper Saddle River, NJ, 2003.

[Gor02] M. Goresky, "Fibonacci and galois representations of feedback-with-carry shift registers," *IEEE Transactions on Information Theory*, vol. **48**, pp. 2826 – 2836, 2002.

[Lib99] J.C. Liberti and T.S. Rappaport, *Smart Antennas for Wireless CDMA Communications*, Prentice Hall, New Jersey, 1999.

[Sch86] R. O. Schmidt, "Multiple emitter location and signal parameter estimation," *IEEE Transactions on Antennas and Propagation*, vol. **AP-34**, no. 3, pp. 276–280, March 1986.